ELSEVIER

Contents lists available at ScienceDirect

# Composites Part A

journal homepage: www.elsevier.com/locate/compositesa





# A novel tooling-free carbon fibre reinforced polymer (CFRP) manufacturing method, double point incremental forming (DPIF) with direct electrical curing (DEC)

Yunlong Tang\*, J. Patrick A. Fairclough

The School of Mechanical, Aerospace and Civil Engineering, The University of Sheffield, Sheffield S1 4DT United Kingdom

#### ARTICLE INFO

#### Keywords:

Double point incremental forming(DPIF)
Direct electrical curing (DEC)
Mould-free manufacturing
Carbon fibre reinforcement polymer (CFRP)
Cost-effective
Environmentally friendly

#### ABSTRACT

Carbon fibre-reinforced polymers (CFRPs) are essential in various industries due to their exceptional specific mechanical properties. However, conventional CFRP manufacturing involves significant costs related to moulds, ovens, and autoclaves, rendering it expensive for low-volume production and prototyping. This study introduces a novel method, Double-Point Incremental Forming with Direct Electric Curing (DPIF-DEC), which enables CFRP fabrication without the need for moulds, directly from CAD models, but it is not suited for mass production. This technique, enhanced by the addition of 2 wt.% carbon black to the epoxy resin matrix, improves through-thickness electrical conductivity, allowing uniform and rapid curing. DPIF-DEC demonstrates rapid localised curing, real-time process monitoring, and achieves mechanical properties comparable to traditional methods. Additionally, it reduces energy consumption, presenting a cost-effective and environmentally sustainable solution for low-volume and prototype CFRP production, laying the groundwork for future applications in continuous-fibre composite manufacturing directly from CAD models.

#### 1. Introduction

Carbon fibre-reinforced polymers (CFRPs) have extensive applications across diverse sectors, including aerospace [1], automotive [2] and construction [3]. Though CFRPs can be manufactured by various methods, most require "tooling", i.e. moulds and substructures to support the mould. Moulds are essential for defining the shape of the composite. They can be constructed from wood or epoxy resin for low-volume applications and from aluminium, steel, or other metals for extended service life for high-volume production. Metal moulds are expensive, but the long service life offsets these costs. However, for low volume or prototyping, a custom mould is often prohibitively expensive [4]. Consequently, for prototype, low-volume or custom CFRP products, the mould cost typically represents the largest investment, leading to significant expenses for prototyping. It is compounded by environmental and economic concerns associated with the disposal of the moulds.

Alternative and innovative manufacturing techniques have been explored to overcome the above issues. Additive manufacturing (AM) is one such novel manufacturing method. Additive manufacturing can manufacture CFRP parts directly without the necessity for moulds. A wide variety of production processes have been used, such as fused

filament fabrication [5,6], laminated object manufacturing [7], and composite-based additive manufacturing [8]. However, these methods have limitations, such as low fibre volume fraction [5,9], high void rate [10–12], or simple layups that do not allow the fibre direction to be tailored to complex stress fields [9,13]. Here, we present Double-Point incremental Forming (DPIF) as an alternative to these processes, providing design flexibility, higher fibre volume fraction and the ability to tailor the fibre direction to the design stresses.

In response to the above challenges, single-point incremental forming of composites (SPIF) has been proposed. Initially, SPIF was used in ductile sheet metal forming [14–16]. The workpiece is securely clamped above a net-shape mould (open mould method). A tool or stylus, whose motion is governed by a computer numerical control (CNC) system, incrementally shapes the workpiece until the desired form is achieved [17]. This technology has been extended to composite systems. Emami et al. [18] employed SPIF in conjunction with a ceramic infrared heater positioned beneath the sample to fabricate unidirectional (UD) glass fibre-reinforced (GFRP) polyamide 6 (PA6) sheets. Their findings indicated that elevating the moulding temperature and reducing the fibre volume fraction enhanced the formability of composite sheets. In addition, the moulding performance of composite sheets with fibre

E-mail addresses: ytang52@sheffield.ac.uk (Y. Tang), p.fairclough@sheffield.ac.uk (J.P.A. Fairclough).

<sup>\*</sup> Corresponding author.

orientations of 0°/90° is significantly inferior to that of unidirectional fibre composite sheets. Okada et al. [19] reported SPIF of CFRPs using forming punches and localised optical heating. Their result demonstrated that the heater significantly influences the deformation of CFRPs, mainly when the sample thickness is low. Cedeno-Campos et al. [20] used a heated copper tool positioned by a CNC system to manufacture thin-section CFRPs. The system used force feedback control to ensure a uniform consolidating pressure on the samples. The result reported that the mechanical properties of these parts were equivalent to those of traditional manufacturing methods (oven, hotpress and autoclave). However, the poor thermal conduction through the CFRP limited the production rate and panel thickness. Compared with conventional manufacturing methods, SPIF often uses a single net-shape open mould to replace two closed moulds, which can significantly reduce costs. In addition, SPIF can directly heat the samples and significantly reduce energy costs, especially for small samples and short production runs [18,20]. As a result, SPIF is increasingly popular in small-scale manufacturing.

Though SPIF effectively reduces mould costs, it still necessitates using a mould (open mould). Double-point incremental forming (DPIF) is proposed to achieve truly mould-free manufacturing. In DPIF, the mould used in SPIF is substituted by an additional forming tool. DPIF has been successfully employed to manufacture sheet metal parts with complex geometries [21]. Though the application of DPIF in sheet metal forming is mature [21,22,23], its use in FRP manufacturing is novel.

To overcome issues concerning heat conduction in DPIF, direct electric curing (DEC), or Joule heating, passes an electric current between the two tools, establishing a rapid yet uniform heating profile through the thickness of the laminate. Carbon fibre is inherently conductive and acts as its heating element. To further improve electrical conductivity and heat distribution, conductive low-cost carbon black (CB) nanoparticles were added to the epoxy resin [24,25] to create a conductive matrix. Thus, DEC can be leveraged to produce a low-energy, highly controllable curing process that directly heats the composite part through its entire thickness [26–29]. In addition, previous research on electrical curing indicated that the sample achieves the optimal temperature distribution and lowest energy consumption when electrical current flows through the ply stack perpendicular to the fibre direction, compared to other electrode contact arrangements [29].

This work used DPIF-DEC to manufacture CFRPs with 2 wt.% CB in the matrix. Previous studies indicate that compared to other electrode contact methods, DEC achieves more uniform and rapid curing when current flows perpendicular to the fibre direction through the ply stack [29]. The key advantages of the DPIF-DEC method include the production of rapid localised curing, controlled degree of cure (DoC), and low energy consumption during the curing process. In this work, flat panel samples were prepared; this is motivated by the need for flat panels in the mechanical testing protocols. It also simplifies the control algorithms and reduces the out-of-plane mechanical forces on the low-cost CNC frame. The total cost of CNC, including the modification cost, is less than 1200 lb. Compared with RTM, DPIF has an inherent flexibility. In terms of RTM, when manufacturing different products, the required moulds are different. Depending on the size, profile, and material of moulds, the cost of moulds can reach a few thousand pounds. As a result, DPIF is beneficial for prototype, low-volume or custom CFRP products. It can reduce the cost of moulds, which is a significant percentage of the total manufacturing cost. Future work will create parts formed into curved parts using more flexible robotic systems.

## 2. Materials

In terms of CFRP, the matrix epoxy resin is an insulator. The addition of the CB creates a conductive matrix that is required for the electric cure. In the previous research [29], the resistivity of CFRP containing 2 wt.% CB in the matrix is reduced to 75 % of that of unmodified CFRP, decreasing from 240  $\Omega\cdot\text{cm}$  to 180  $\Omega\cdot\text{cm}$ . As a result, CFRP with 2 wt.%

CB in matrix is used in this project.

#### • Epoxy resin system

The epoxy resin is IN2 epoxy infusion resin from Easy Composites Ltd (UK), from Easy Composites Ltd (UK), characterised by its low viscosity, which facilitates the dispersion of nanoparticles. The main components of it are Bisphenol A diglycidyl ether and phenolic epoxy resin F-44. The hardener is AT30 slow (AT30S) from Easy Composites Ltd, which is liquid at room temperature. Its main components are Isophoronediamine and Poly(propylene glycol) bis(2-aminopropyl ether). IN2 resin/AT30S can be cured at room temperature in 24 h. AT 60 °C and 100 °C, it takes 6 h and 3 h, respectively (Supplier's Data [30]). The density of cured IN2/AT30S is  $1.172\pm0.006$  g/cm³, measured by helium pychnometry (AccuPyc II 1340).

#### • Carbon black (CB)

"Carbon black, acetylene, 100 % compressed" was purchased from Thermo Scientific Chemicals and has a density of  $1.8~g/cm^3$  [31]. CB is an agglomerate of 10 nm CB spheres, forming irregular shapes [32].

The density of IN2 resin/AT30S with 2 wt.% CB is  $1.177\pm0.006$  g/cm $^3$  measured by helium pychnometry.

#### • Carbon fibre

The carbon fibre used is 2x2 twill 3 k carbon fibre cloth carbon supplied by Easy Composites Ltd. The carbon fibre is a TR 30S 3L manufactured by PYROFIL<sup>TM</sup>. The filament diameter is 7  $\mu$ m. The manufacturer's data sheet gives the tensile strength and modulus as 4.12 GPa and 234 GPa, respectively [33]. Its areal weight and density are 210 g/cm² and 1.79 g/cm³ respectively [34].

#### 3. Methodology

The relevant information concerning the equipment and techniques employed are summarised in this section.

#### 3.1. Matrix modification and composite manufacturing

This subsection includes three parts describing the CFRP manufacturing process with 2 wt.% CB in the matrix.

#### 3.1.1. Matrix modification

Firstly, 100~g of IN2 resin and 2.7~g of CB were added to a disposable plastic beaker. A wooden spatula was first used to hand pre-mix the mixture for 30~s. Subsequently, the mixture was blended using an overhead stirrer ("Hei-TORQUE Value 100'' from Heidolph Instruments, Schwabach, Germany) for 10~m mia at 900~rm. Following this, 30~g of AT30S hardener was incorporated into the mixture and blended with the overhead stirrer for an additional 3~min at 900~rm. The final mixture was degassed under vacuum degassing before hand layup.

# 3.1.2. Pre-preg composite manufacturing: Hand layup

Pre-preg is a carbon fibre fabric impregnated with a high-viscosity, partially cured resin. Because of the 2 wt.% CB and the small panel size, hand layup was used to manufacture the pre-preg composite panel. This method offers the advantages of being both rapid and cost-effective. However, hand layup suffers from poor repeatability in terms of fibre volume fraction. Consequently, the sample was subjected to vacuum consolidation post-layup to enhance fibre volume fraction while providing a more reproducible fibre volume fraction.

The glass plate was prepared by spraying CR1 Easy-Lease Chemical Release Agent (Easy Composites Ltd, Stoke-on-Trent, UK) onto the glass surface, following the manufacturer's recommended procedure. Then, a  $160 \times 160$  mm carbon fibre sheet was placed on the glass surface, and 2

wt.% CB resin liquid was uniformly spread by hand onto the carbon fibre surface using a brush. These two steps were repeated until either 5 or 15 layers of carbon fibre were stacked for the tensile and four-point bending tests, respectively. Then, a  $170\times170$  mm piece of release film and a vacuum breather fabric were placed on top. Finally, the entire assembly was covered with a vacuum bag and sealed with vacuum tape. The sample was consolidated using a vacuum pump for approximately 15 h overnight at room temperature and then de-moulded to collect the prepreg samples. The DoC of the pre-preg, measured by DSC, was 0.62, which is over the gel point (0.56), but it is not yet glassy. The glass temperature (Tg) of CFRP is about 86 °C (detail in SI). In the future work, the relationship among the deformation degree, thickness, and external force of pre-preg.

#### 3.1.3. Comparative Composites manufacturing methods

Two traditional manufacturing methods, oven and autoclave, were used to compare with DPIF-DEC.

#### Oven

The pre-preg samples (initial DoC, 0.62) were covered by release films and breathers and placed in vacuum bags for oven curing. The samples were cured at 70  $^{\circ}$ C for 3 h in a UT 6200 oven (Thermo Fisher Scientific Inc., USA). The heating and cooling rate was set to 3  $^{\circ}$ C/min. An external vacuum pump maintained vacuum consolidation during curing at a -0.8 bar gauge pressure (0.2 bar absolute).

#### Autoclave

The pre-preg samples (initial DoC, 0.62) were loaded into the autoclave (AC052 Autoclave, Premier Autoclaves, UK), attached to the vacuum hoses, and subjected to a vacuum of  $29^{\prime\prime}$  Hg (approximately 1 bar). The autoclave was then sealed, pressurised to 6 bar, and heated at a rate of 3 °C/min to 70 °C, where the samples were cured for 3 h.

# DPIF-DEC machine

DPIF used incremental curing with localised Direct Electric Curing (Joule Heating). DPIF involves two primary steps. First, a  $300\times300$  mm aluminium plate supported the uncured CFRP pre-preg with a  $150\times150$  mm cut-out. The pre-preg sample was clamped using Teflon bolts and Teflon bars to isolate it from the aluminium plate electrically (Fig. 1 (a)).

Secondly, the surface of the two 20 mm diameter copper tools was wipped twice with CR1 Easy-Lease Chemical Release Agent (Easy Composites Ltd, Stoke-on-Trent, UK). Then, the copper tools compressed the upper and lower surfaces of the pre-preg (Fig. 1 (b)). These 20 mm tools were supplied with DC electrical power via a PS1540S SMPS bench power supply (Rapid Electronics, Colchester, UK). The tool temperature is monitored by type K thermocouples embedded within the copper tools and recorded using a Picolog TC-08 data logger (see Fig. 1 (b)). Two 500 N load cells (LCM System, UK) were connected to the copper tools to

measure the forces exerted by the tools on the pre-preg. The signals from the load cells were acquired using a cDAQ-9171 Compact DAQ (National Instruments). The motion of the tools was controlled by two XYZ Cartesian machines driven by MT-2315HS300AW-C stepper motors (MOTECH MOTOR, China). The communication between stepper motors and PC software (LabView) is via a CNC controller (X-Pro V1). The components and structure are shown in Fig. 2.

In the curing process, the upper and lower tools were first aligned coaxially and brought into direct contact with the CFRP pre-preg sample. The top tool pressed the fixed pre-preg sample with a 0.4 mm/s incremental step in the z-direction until a 160 N load (5 bar) was achieved. DC was applied, raising the temperature within the CFRP. The temperature at the copper tool (see section 3.2) was controlled at 50, 60, 70, or 80 °C to cure a single point and determine the optimal curing temperature. This optimal tool temperature, 80 °C, was then used to manufacture the CFRP plate sheet. (It should be noted that this tool temperature is far below the actual temperature of the CFRP below the tool). Subsequently, the tools were separated and moved 10 mm (half the diameter of the tools) in the +x-direction to the next curing point. Each step takes 90 s from the start of one step to the beginning of the next. This process was continued until the desired x-distance (110 mm) was reached. At the end of the x-translation, the tool was moved 10 mm in the +y-direction, and the above process was repeated, but now the tool is moving backwards, in the -x-direction. This process was repeated across the entire sample, requiring 3-4 h to complete the process and cure the composite.

#### 3.2. Temperature rise during the DPIF process

Tests were conducted to correlate the measured tool temperature with the sample temperature. Three type K thermocouples were placed within the sample at the top, middle, and bottom positions, 30 mm away from the starting curing point. Fig. 1 (b) shows a schematic of this thermocouple arrangement. In addition to the thermocouples, an E4 thermal imaging camera (FLIR Ltd., US) was used to image the temperature distribution on the sample surface during the curing process.

#### 3.3. Experimental testing and analysis

#### 3.3.1. The degree of cure (DoC)

The cure profile and DoC were examined by DSC (PerkinElmer DSC 4000) [34]. Samples were collected from uncured resin, the edge and centre of the cured laminates by waterjet cutting, and from these, DSC samples of around 10 mg were cut by hand. The DSC heating cycle, ranging from 40 °C to 250 °C at a rate of 10 °C/min, was used to determine the DoC. For the uncured resin, the same temperature range was used with four different heating rates:  $10\,^{\circ}$ C/min,  $15\,^{\circ}$ C/min,  $20\,^{\circ}$ C/min, and  $25\,^{\circ}$ C/min, which allowed the cure kinetics at different heating rates to be determined. Here, the temperature rate we used is far lower than real increase rate of temperature (90 °C/min) in DPIF. The issue with the higher DSC heating rates is that it is difficult to separate the

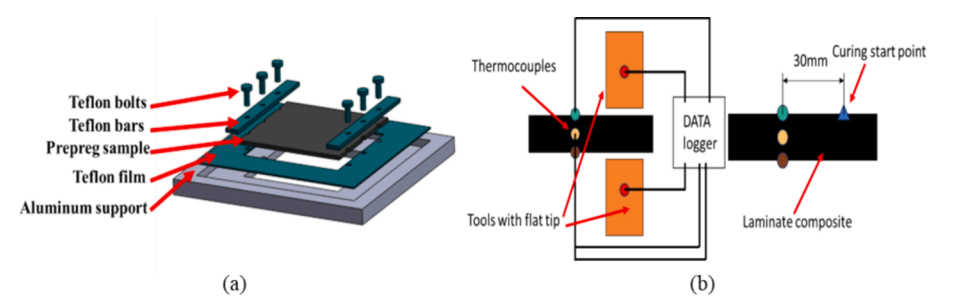


**Fig. 1.** (a) The sample clamp for DPIF and fabric arrangement. (b) The schematic of the thermocouple locations. The thermocouple locations are the green, beige and brown circles in the black sample and red circles in the DPIF copper tools, 10 mm away from the surface that contacts the fabric. (For interpretation of the references to colour in this figure legend, the reader is referred to the web version of this article.)

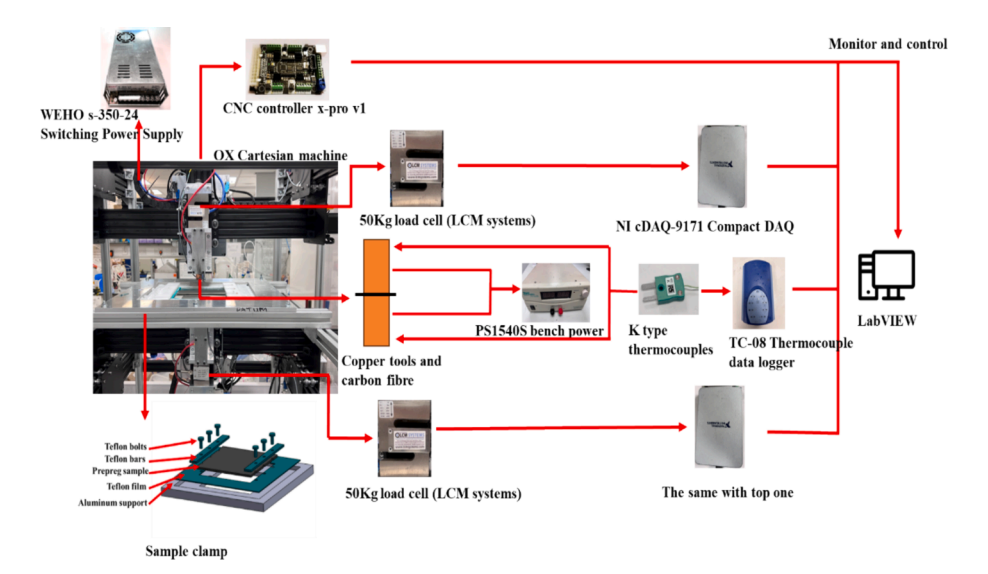


**Fig. 2.** The component and structure of DPIF (the red arrows represent physical connections between elements). (For interpretation of the references to colour in this figure legend, the reader is referred to the web version of this article.)

enthalpy of the curing reaction from the baseline on our DSC instrument, and the DSC baseline can significantly change the results. In addition, the difference of DoC value calculated by kinetic model and real DoC value measured by DSC machine is small. As a result, the kinetic model can provide practical and sufficiently accurate results in predicting the curing process.

#### 3.3.2. The Arrhenius equation to model cure kinetics

Since the curing process of CFRP involves non-isothermal kinetics, an n-th order kinetic model (Eq. (1) and the Arrhenius equation (Eq. (2) were employed to measure the DoC as a function of temperature and time [35]. The Kissinger equation (Eq. (3) was employed to calculate the activation energy ( $E_a$ ) and pre-exponential factor (A). Finally, the Crane equation (Eq. (5) was used to determine the order of the reaction (n) [36].

$$\frac{d\alpha}{dt} = k \bullet (1 - \alpha)^n \tag{1}$$

$$k = A \bullet e^{\frac{E_a}{R \bullet T}} \tag{2}$$

Where k is the rate constant; n is the reaction order; R is the gas constant [8.314 J/(mol K)]; T is the temperature in Kelvin;  $\alpha$  is the degree of reaction, and t is the time in seconds.

#### • Kissinger equation

The Kissinger equation (Eq. (3) was used to calculate the parameters of the Arrhenius equation [37]. When n is close to 1, the model more accurately represents the data. For a given DSC curve with a heating rate  $(\beta)$ , the peak temperature  $(T_p)$  at the maximum reaction rate is first determined. A Kissinger plot can then be obtained by plotting  $\ln(\beta/T_p^2)$  against  $1/T_p$  for a series of DSC curves with different heating rates. The slope of the Kissinger plot can be used to determine A and  $E_a$  from the slope and intercept, respectively.

$$\ln\left(\frac{\beta}{T_p^2}\right) = \ln\left(\frac{A \bullet R}{E_a}\right) - \frac{E_a}{R \bullet T_p} \tag{3}$$

#### • Crane equation

When  $E_a/(n \cdot R) \gg 2T_p$ , the Crane equation (Eq. (4) can be simplified

as in Eq. (5), where the value of n can then be calculated by the slope of the fit line in  $\ln(\beta)$  against  $\ln(1/T_p)$ .

$$\frac{d(\ln\beta)}{d(T_p^{-1})} = -\left(\frac{E_a}{n \bullet R} + 2T_p\right) \tag{4}$$

$$\frac{d(\ln \beta)}{d(T_p^{-1})} = -\left(\frac{E_a}{n \bullet R}\right) \tag{5}$$

## 3.3.3. Physical properties of CFRP samples

Density was determined by helium pycnometry (AccuPyc II 1340, Micromeritics Ltd, UK) and a density balance. The purge and cycle fill pressure was set to 19 psig (1.31 bar). Each sample was measured five times. The volume and mass fractions ( $V_f$  and  $W_f$ ) of fibre were determined using the densities of the laminate, matrix and carbon fibre. A density balance with pure water was used to measure composites' bulk density ( $\rho_b$ ) via the Archimedes principle (ISO 1183–1:2019). This method does not account for the voids within the composite. However, the density measured by AccuPyc II 1340 uses Helium and thus fills voids that are connected to the surface (pores), which follows the standard ASTM D4892. This density can be regarded as real composite density,  $\rho_c$ . As a result, the void volume fraction can be determined as  $\Phi$ = 1-( $\rho_b/\rho_c$ ). The most significant uncertainty in this is likely to be the bulk density,  $\rho_b$ . The presence of air trapped on the surface or incomplete wetting of the sample leads to a reduction in this value. Thus, the void fraction presented should be regarded as an upper limit.

# 3.3.4. The numerical analysis of the curing process in DPIF

A numerical analysis using Abaqus was conducted to determine a more representative model of the curing area and temperature distribution in the experiment. For the numerical analysis, a  $120 \times 120 \times 4$  mm (L×W×T) geometry was selected. The meshing was course and not plyby-ply as the FEA is to simulate the curing and not the mechanical properties, and thus ply-by-ply increases computational cost. The numerical analysis (Abaqus) examined the temperature distribution during the DPIF process, considering heat transfer due to heat conduction between heated and adjacent areas, as well as the exothermic curing reaction of the resin. Here, to simplify the calculation of heat input from DEC and the heat loss of copper tools, we fix the surface temperature of the sample at the cure point based on the experimental thermocouple measurement.

The material properties of CFRP are shown in Table 1. The density is from Table 4. The thermal properties, including heat capacity  $(C_p)$  and

**Table 1** The material properties of CFRP used in the numerical analysis (Abaqus). Values for  $k_{11}$  and  $k_{22}$  are taken from literature [39,40].

Density $\rho_c$ (kg/m <sup>3</sup> )	Thermal capacity $C_p$ (J/ (kg·k))	Thermal conductivity $k$ (W/ $(m \cdot K)$ )
1420	1440	$k_{11} = 7, k_{22} = 7, k_{33} = 0.48$ $k_{12} = 0.3, k_{13} = 0.3, k_{23} = 0.3$

thermal conductivity, through the sample thickness ( $k_{33}$ ), were measured using the LFA 467 Hyper Flash (NETZSCH, Selb, Germany). The thermal conductivities along the fibre ( $k_{11}$  and  $k_{22}$ ) were referenced from the literature [38]. The thermal conductivities,  $k_{12}$  and  $k_{23}$  were assumed to be equivalent to the conductivity of the resin [39].

To simulate a step in the DPIF process, the upper and lower surface temperatures of a 20 mm diameter circle were varied in accordance with the thermocouple data (section 4.4.2), increasing from 40  $^{\circ}\text{C}$  to 170  $^{\circ}\text{C}$  in 90 s, where the temperature of copper tool is controlled at around 80  $^{\circ}\text{C}$  (see Table 3). The heating path was the same as that of the tools in the DPIF experiment. Several simplifications were applied in this model. The heat transfer between the tool and sample was assumed to be perfect, and the moving time of the tools between unit heat circles was set to zero. The heat transfer from the heating area into the adjacent material and the exothermic reaction of the resin during curing were considered.

#### 3.3.5. Tensile properties

In terms of CFRP with a woven fabric, the tensile properties are predominantly influenced by the fibre's tensile properties. Therefore, tensile tests following the ASTM D30309 standard were conducted to determine if DFIP degrades the fibre in any way. An H25Ks Benchtop Tester (Tinius Olsen, USA) was used with a 25 kN load cell. The displacement rate was set to 1 mm/min. The strain values were recorded using a Pike F-505B/c (LIMESS Messtechnik, Germany) DIC camera. Specimen dimensions of  $150\times15\times1$  mm (L×W×T) were used due to the size limitations of the DPIF sample holder.

#### 3.3.6. Flexural properties

Four-point bending tests were conducted using an H25Ks Benchtop Tester (Tinius Olsen, USA). The dimensions of the test specimen and the testing conditions were determined according to the ASTM D7264 Standard. The dimension was  $80\times13\times\sim4$  mm (L×W×T). The displacement rate was set to 1 mm/min.

# 3.3.7. Energy consumption measurements

A single-phase in-line Power Meter (Intertek, UK) was used to record the energy consumption of the oven and DPIF during the curing process. The energy consumption of the autoclave is measured by RI-70–100-P, a 3-phase in-line power meter (Rayleigh Instruments, UK).

# 4. Results

The purpose of the project is to examine the DPIF manufacturing for thick CFRP samples. As a result, all curing process analyses focus on 15 layers CFRP samples. The 5 layers of CFRP samples are used for fibre damage detection, which is tested by the tensile tests, and energy consumption comparison in the curing process.

#### 4.1. Cure modelling

This section develops a function describing the curing reaction using the Kissinger and Crane equations with data from DSC.

#### 4.1.1. DSC of the matrix

The DSC curves of IN2/AT30S resin are shown in Fig. 3. As expected, with increasing heating rate, the exothermic peak narrows. The  $T_p$  and maximum heat flow increase.

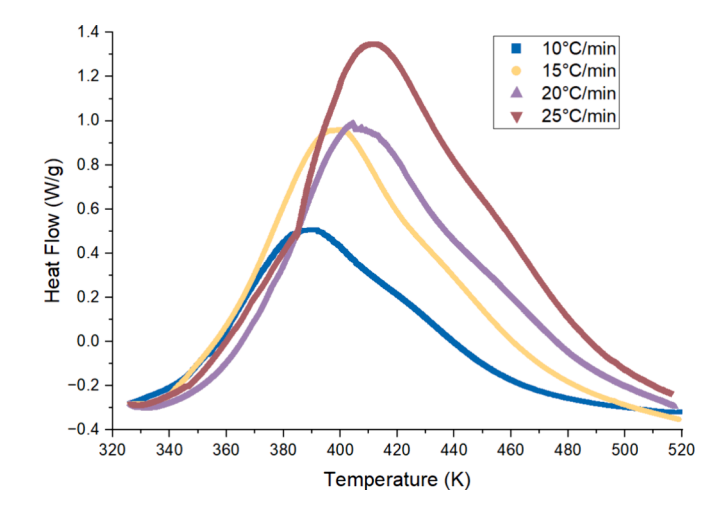


**Fig. 3.** DSC curves of IN2/AT30S resin at different heating rates. (Showing the peak temperature,  $T_p$ , moving to a higher temperature with an increased heating rate.).

# 4.1.2. Kissinger equation

Schultz describes how the relevant kinetic parameters can be determined from DSC for the Kissinger equation [37]. These results are shown in Table 2. The plot of  $\ln(\beta/T_p^2)$  against 1000/Tp is shown in Fig. 4 (a). The Ea and A values can be calculated from this data as 52.9  $\pm 6.2$  kJ/mol and  $0.48\pm 0.06\times 10^6$  s<sup>-1</sup>, respectively.

#### 4.1.3. Crane equation

The Crane equation is used to determine the order of reaction, n. The plot of  $\ln(\beta)$  against  $1/T_p$  and its corresponding fit is shown in Fig. 4 (b). The determined value of n is  $0.97\pm0.02$ . For non-isothermal cure kinetics, the value of n is expected to be close to 1.0 [41,42]. (For isothermal cure kinetics, the value of n is seen to be close to 2.0 [43,44] In this project, the curing temperature is variable so that non-isothermal cure kinetics can be applied.

As a result, the curing reaction model can be built as Eq. (6).

$$\frac{d\alpha}{dt} = 0.48 \bullet 10^6 \bullet e^{\left(\frac{52.9 \bullet 10^3}{8.314 \bullet T}\right)} \bullet (1 - \alpha)^{0.97}$$
 (6)

## 4.2. The influence of the curing temperature on the DoC

Table 3 presents the "surrounding" temperature, DoC, and cure point temperature. The surrounding temperature, as measured by an IR camera, is the temperature of the CFRP adjacent to the tool. The camera cannot measure the temperature under the tool as the tool obscures this area. The curing reaction function was used to estimate the cure point temperature (Eq. (6) based on curing time and the DoC measured after curing. Here, the cure point temperature is assumed to be a constant value during the curing process. When the temperature of the copper tool was measured at 70 and 80 °C, the cure point temperature, directly under the tool, was predicted to reach around 160 °C. The DoC value was expected to rise from the initial pre-preg value of 0.62 to over 0.93 within 90 s of the tool passing current through the pre-preg. The cure point temperature was assumed to be constant. However, due to the

**Table 2**The kinetic parameters of curing reaction for the different heating rates.

Speed rate β (°C/min)	Peak point temperature $T_p$ (K)	$1000/T_p$	$\ln(\beta/T_p^2)$
10	390.39	2.56	-9.63
15	401.30	2.49	-9.28
20	404.65	2.47	-9.01
25	411.37	2.43	-8.82

**Table 3**The surrounding temperature, DoC, and cure point temperature at different set temperatures.

Copper tool temperature (°C)	Surrounding D temperature from IR camera (°C)		Modelled Cure point temperature (°C) (Eq. (6)
80	145	0.95	160
70	125	0.93	155
60	95	0.77	120
50	64	0.65	85

rapid temperature increase during the curing process and the slow response of the tool thermocouple, the actual maximum temperature at the cure point is probably higher. A maximum tool temperature of 80  $^{\circ}$ C was maintained for the curing process to ensure maximum cure without damaging the matrix. The validity of the cure point temperature data is further examined in section 4.4.2.

#### 4.3. The consolidation load changes during the DPIF process

Fig. 5 shows the changes in consolidation load during the curing process for 15 plies laminate when the copper tools press the sample to an initial force of 160 N and the position is held. As the composite is cured, the volume of the epoxy resin decreases. It is commonly termed chemical or cure shrinkage [45]. If the external tools are kept at fixed positions during this process, the external stress will reduce as this shrinkage occurs (the force scale is negative). This shrinkage is limited, as the change in this force is only about 6 %. The change in force over time provides an indirect measure of the curing process. Though it does not provide a reliable measure of DoC, it is sufficient to indicate that the tools can move to the next step in the process. The enlarged view in Fig. 5 shows the force data of a single point during cure, which shows that after 1 min, the force curve flattens, indicating that the DoC of the sample is high and the volume change is minimal. Therefore, the tool can move to the next point, and the process is repeated.

#### 4.4. The temperature changes during the DPIF process

In this section, the temperature changes of the copper tools and the CFRP sample are examined during the DPIF process.

#### 4.4.1. The temperature changes of the copper tools

Fig. 6 shows the temperature changes, as measured by the thermocouples in the tools, during the DPIF process. In the first 20 min, the temperature increases from room temperature to 80 °C and 70 °C for the upper and lower tools, respectively. Then, the temperature was manually controlled at 70–90 °C for the upper tool and 60–80 °C for the bottom tool by varying the current. The upper tool (cathode) is expected to be at a higher temperature due to the junction bias [29,46,47]. The temperature quickly decreased when the tools were moved away from

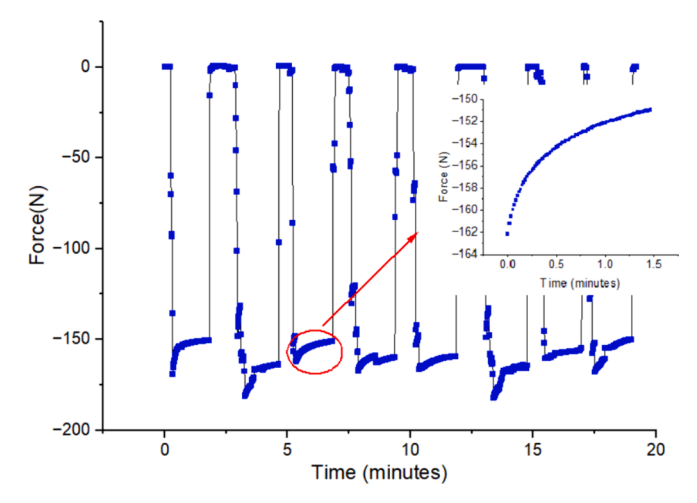


Fig. 5. The load change during the DPIF process for 15 plies laminate in the first 60 min.

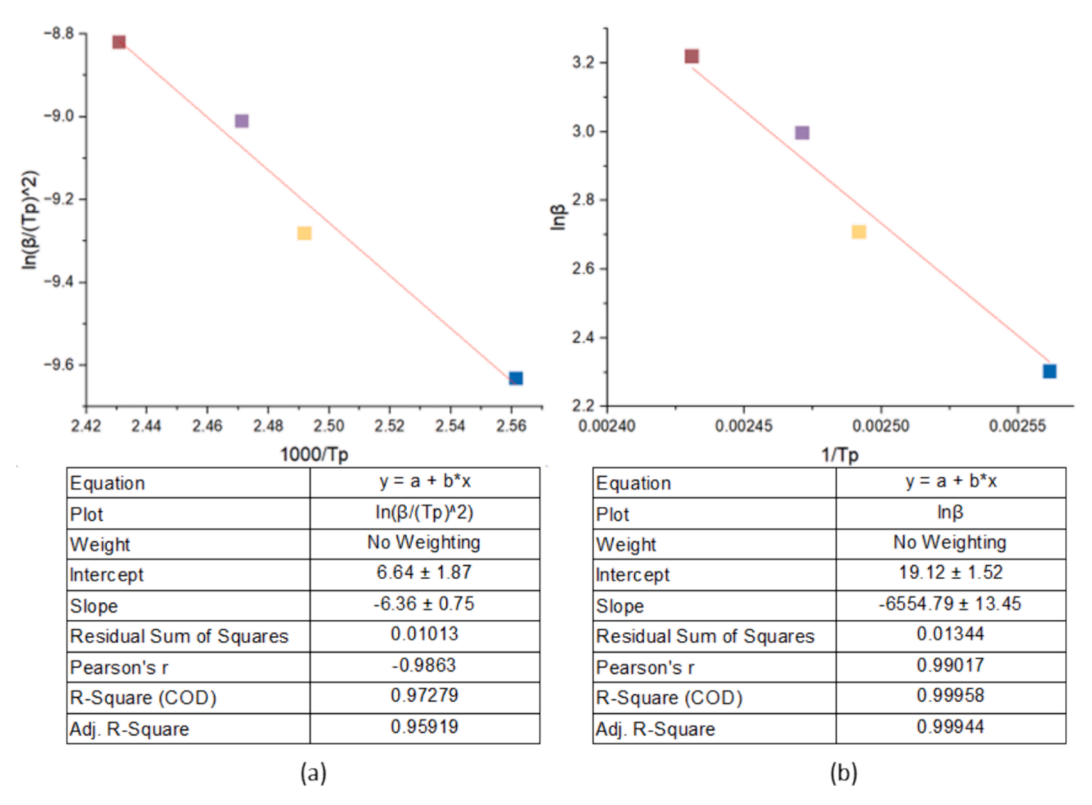


Fig. 4. (a) The scatter plot of  $\ln(\beta/T_p^2)$  against  $(1000/T_p)$ . (b) The scatter plot of  $\ln(\beta)$  against  $(1000/T_p)$  with their fit line and fit information.

Y. Tang and J.P.A. Fairclough Composites Part A 187 (2024) 108478

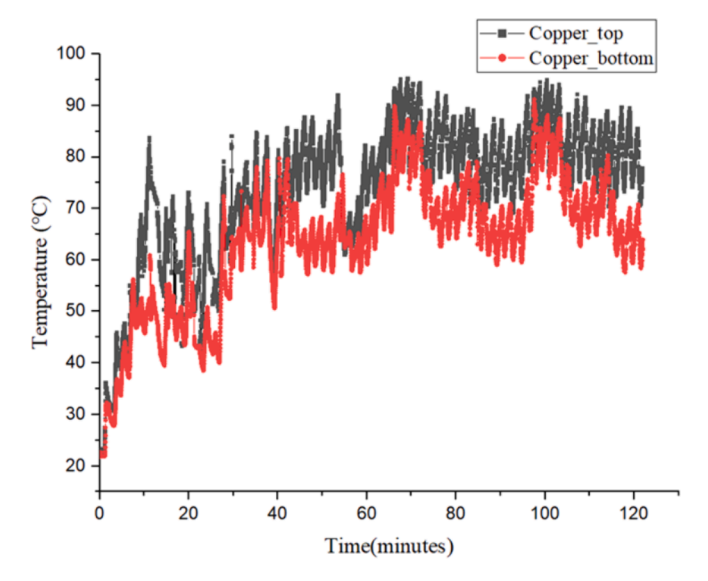


Fig. 6. The temperature changes of copper tools during the DPIF process in the first 120 min.

the sample, as no current was flowing.

#### 4.4.2. Cure point temperature data

Fig. 7 (a) shows the temperature changes at the top, middle, and bottom thermocouples embedded in the sample (15 layers). The tool starts at a point approximately 30 mm in the x-direction from these thermocouples. In the first peak area, the temperature shows a rapid increase, whose average increase rate is about 85 °C/min. This data is used in Abaqus for numerical analysis. The red circle in Fig. 7(a) shows where the copper tools directly contacted the (electrically insulated) thermocouple, whereas in the blue circle, the tools passed close to the thermocouple. In Fig. 7(b), the thermocouples show both a rapid temperature rise (130 °C/min) and a rapid cooling (100 °C/min) for top surface in sample. The maximum temperatures of the top, middle, and bottom positions are 185, 164, and 173 °C, respectively. As a result, the sample is rapidly heated throughout its thickness, DoC in the z-direction is uniform (see section 4.5), the sample thickness can be considerably improved, and the cycle time reduced. This result represents a considerable advance over our previous work using heated tools [20]. Due to the junction bias, the top surface temperature is higher than the bottom surface [29], which is discussed in section 4.4.1. The contact resistance between the copper tools and the sample surface leads to the surface temperatures being higher than the middle.

# 4.5. DoC changes during DPIF

From the curing reaction model (Eq. (6) and the temperature profiles in Fig. 7, the changes in DoC during the DPIF process in 15 layers CFRP sample can be modelled, as shown in Fig. 8. The data is clos to the real DoC, 0.95 (see Fig. 14). As a result, this DoC analysis depending on kinetic model is valid. When the pre-preg was prepared, it was left to cure at 20 °C for 16 h overnight. As a result, the DoC had an initial value of 0.62 before the DPIF-DEC process. During the curing process, there are two rapid rises in DoC, which are marked by the red and blue circles, corresponding to those in Fig. 7(a). In the first period, when the copper tools directly contact the fixed point, the DoC at the surface rapidly rises to over 0.9 and the DoC in the middle to 0.85. When the tool moves through one loop and returns to a position close to the fixed point, the

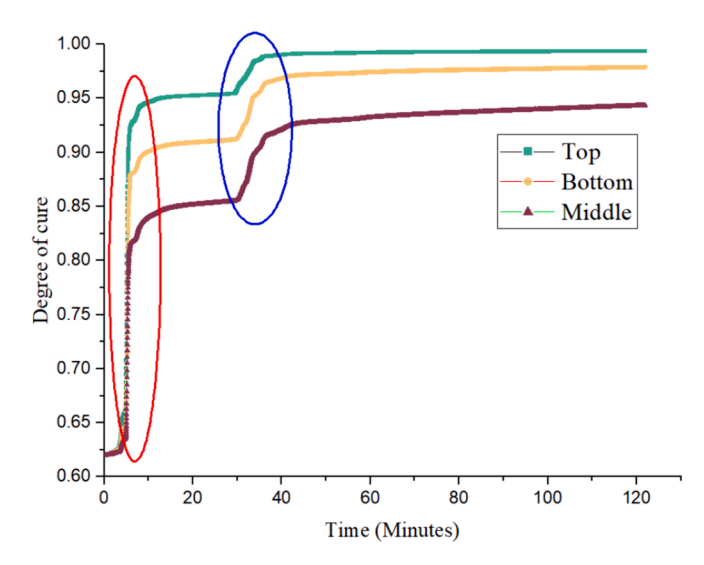


**Fig. 8.** The DoC changes at the top, middle, and bottom positions of a fixed point in the sample, which is about 30 mm in the x-direction from the start point during the DPIF process in 15 layers CFRP sample. The DoC is calculated based on the determined non-isothermal cure kinetics and the temperature history.

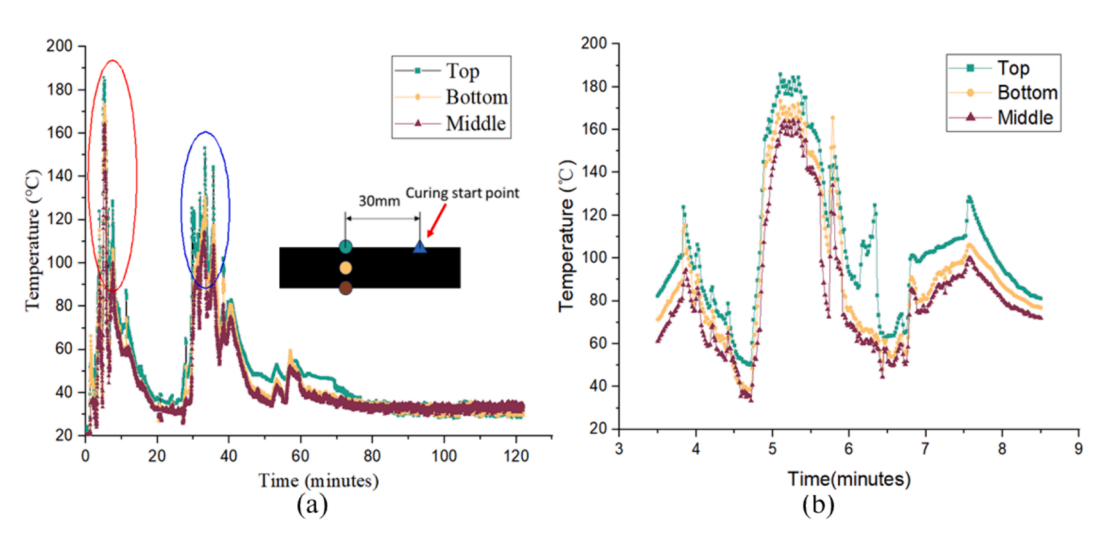


**Fig. 7.** (a) The temperature recorded by the thermocouples at the top, middle, and bottom position of a fixed point in the sample (15 layers), which is 30 mm in the x-direction from the start point during the DPIF process. (b)The magnified image for the red circle in Fig (a) is from 3.5 to 8.5 min. (For interpretation of the references to colour in this figure legend, the reader is referred to the web version of this article.)

DoC increases to over 0.9 for all positions. There are opportunities here to decrease the cycle time by reducing the time at any given point and increasing the spacing of the points. Using a post-cure cycle in an oven with a slow temperature ramp could also improve the production rate for higher volumes. While this would improve production rate, it would also increase energy costs.

#### 4.6. Validation of the cure model

# 4.6.1. The temperature and cure profile under the tool

The time evolution of temperature at a fixed point 30 mm from the start position is shown in Fig. 9. The simplified numerical analysis and experiment temperature data are shown as the blue, open symbols, and the red, closed symbols, respectively. This numerical analysis result is used to estimate the temperature change and DoC during the DPIF process. The simulation cannot effectively model heat loss, as evidenced by comparisons of the cooling profiles between 15 and 25 min and after 40 min in Fig. 9.

Fig. 10 compares the DoC from the experimental temperatures and the numerical analysis. The curing model (Eq. (6) calculated the DoC based on the temperatures and time. The experimental data (red points) shows that as the tool approached the point where the thermocouple was embedded, there was some pre-cure (about 0.62 and 0.65 in DoC) for the two points adjacent to the thermocouple, Fig. 10. Here, the fibre direction influences the thermal conductivity, and for this, 2x2 twill weave, the  $0/90^{\circ}$  tows aligned along the tool path in x- and y- directions contribute to this effect. When the tool is directly above the thermocouple, the temperature rises from 40 to 160 °C in 13 s. Based on the kinetic model, the cure rapidly rises from 0.66 to 0.92 within 40 s.

In the numerical model (blue points), DoC, based on the modelled temperature, rapidly increases and approaches 1 within 270 s. Some inflexion points are noticeable in the model line (blue), but they are not as straightforward as in the experimental (red) data. The DoC is higher in the model, as expected from the higher average temperatures shown in Fig. 9. The difference in DoC indicates that the numerical analysis did not effectively account for heat loss and the movement time of copper tools. It is best illustrated in the data between 10 and 20 min in Fig. 9. In addition, the real DoC data measured by DSC machine in Fig. 14 can prove this analysis is valid.

# 4.6.2. Curing temperature under the tool: IR data and numerical model Fig. 11 shows the temperature distribution of the sample during the

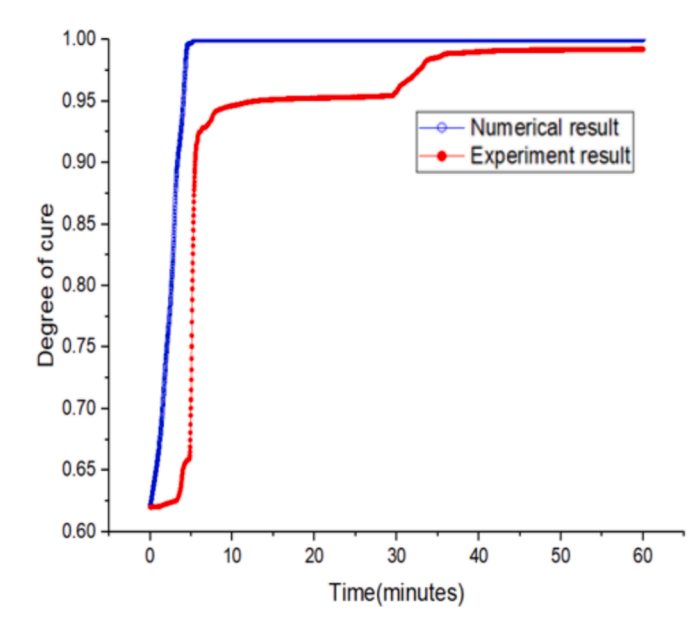


**Fig. 10.** The DoC changes at the fixed point during the DPIF process, which is measured by the experimental (red closed symbols) and simulation (blue open symbols). (For interpretation of the references to colour in this figure legend, the reader is referred to the web version of this article.)

DPIF-DEC process, as measured by the thermal imaging camera (Fig. 11 (a)) and the numerical analysis (Fig. 11 (b)). Fig. 12 presents the numerical model data of the temperature distribution derived from IR images and numerical analysis when the tools are positioned at 60 mm along the x-axis. The movement path of copper tools is shown in Fig. 13. There is no significant difference between the two data sets. As a result, numerical analysis can effectively simulate the temperature distribution close to the heat source. Thus, the numerical model coupled with the IR camera can be used as a control system for effectively monitoring temperature and cure status.

#### 4.7. Cure in the DPIF process, first pass damage

In the DPIF process, the sample is consolidated under pressure, which leads to surface deformation, particularly in the first row of

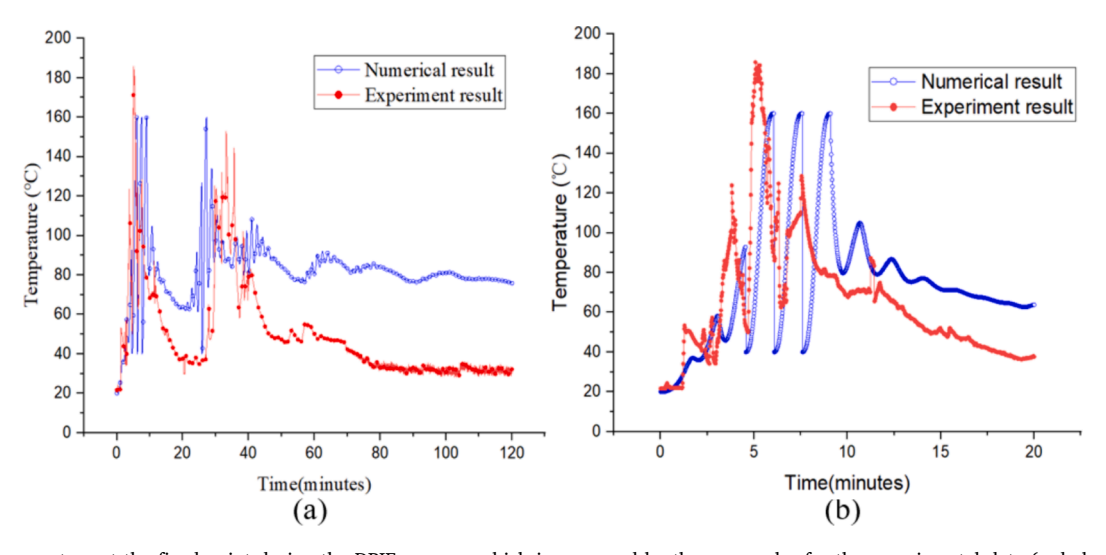
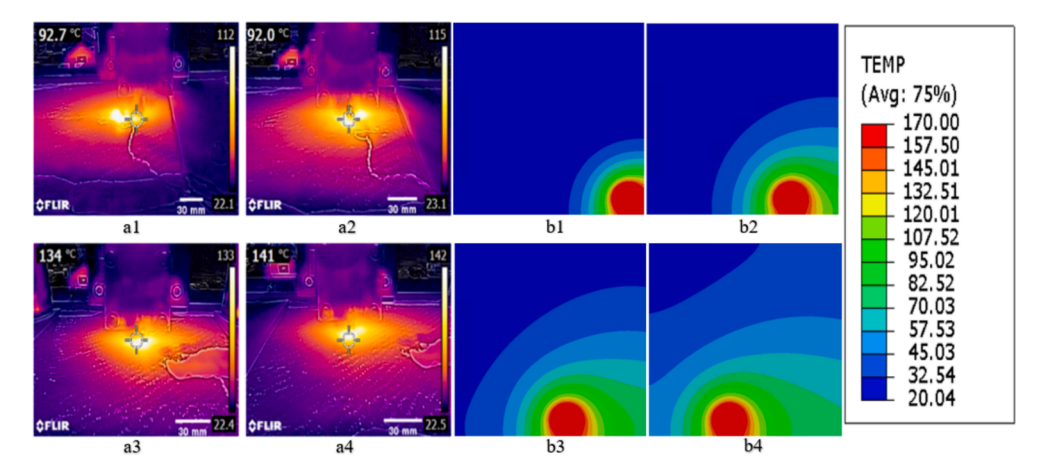


Fig. 9. (a)The temperature at the fixed point during the DPIF process, which is measured by thermocouples for the experimental data (red closed symbols) and simulation (blue open symbols). For clarity, not all the data markers are plotted. (b) A magnified image of Fig (a) shows the repeated passes of the tool that contribute to the high DoC. All data points, at one-second intervals, are plotted. (For interpretation of the references to colour in this figure legend, the reader is referred to the web version of this article.)



**Fig. 11.** The temperature distribution measured by the (a) thermal imaging camera and (b) the numerical result when heating points at (1) 0 mm, (2) 20 mm, (3) 40 mm, and (4) 60 mm. The camera cannot image the area directly beneath the tool, which is the red area in the simulation. The movement of copper tools is from right to left (see Fig. 13). (For interpretation of the references to colour in this figure legend, the reader is referred to the web version of this article.)

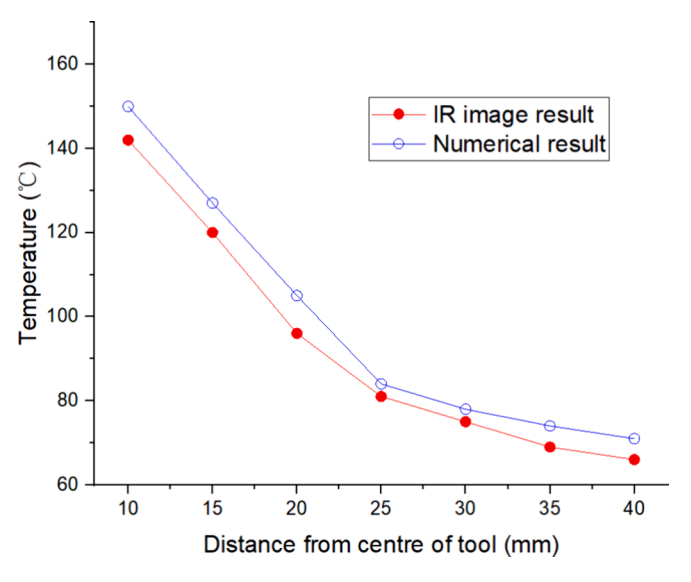
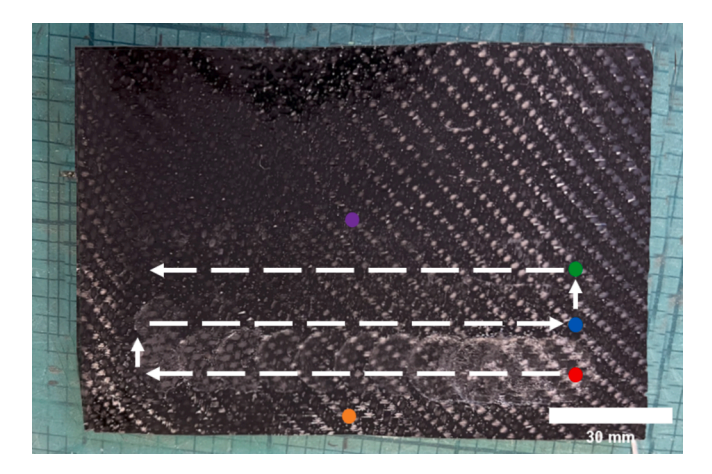


Fig. 12. The numerical data of temperature distribution is derived from the numerical result and IR image results when the heating point is at 60 mm, as shown in image 4 in Fig. 11.



**Fig. 13.** The back profile of the CFRP sample cured by DPIF. The white dashed line with arrows shows the tool path, starting from the red point. (For interpretation of the references to colour in this figure legend, the reader is referred to the web version of this article.)

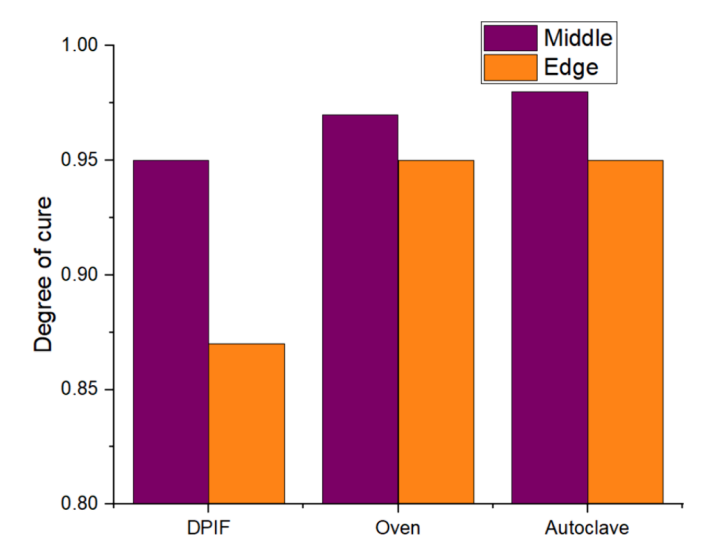


Fig. 14. The DoC of the middle and edge of the samples.

consolidation and curing. Fig. 13 shows obvious deformation at the top (dashed line, starting at the red point), where the tools first contact the sample. However, this deformation is not apparent in the second and later rows in the curing path. Fig. 6 shows that the tool does not achieve the required 80  $^{\circ}$ C curing temperature along this line. Once the tools are at the correct temperature, the marks are no longer present on the second line. In practice, this section is trimmed off as scrap.

#### 4.8. Physical properties

Table 4 compares the physical properties (composite density, volume fraction, and mass fraction of fibre) of DPIF laminates with those manufactured using conventional techniques. Samples manufactured by DPIF have physical properties similar to those produced using traditional manufacturing methods.

#### 4.9. Degree of cure, DoC, variations across the manufacturing methods

Fig. 14 shows the DoC at the middle and edge positions in the samples. The DoC at the middle position in all samples is high, over 0.95. However, the DoC at the edge position (orange circle marked in sample, Fig. 13) in the sample manufactured by DPIF is the lowest among the three manufacturing methods, at only 0.87, which is lower by about 9 %

Y. Tang and J.P.A. Fairclough Composites Part A 187 (2024) 108478

**Table 4**Physical properties of the CFRP samples. The uncertainty is the standard deviation of three samples. The void fraction should be viewed as an upper limit.

Manufacturing methods	Composite density $\rho_c$ (g/ cm <sup>3</sup> )	Fibre volume fraction $V_f$ (vol.%)	Fibre mass fraction $W_f$ (vol.%)	Void fraction <i>Ф</i> (vol.%)
DPIF	$1.42{\pm}0.008$	$39.4{\pm}1.24$	$50.6 {\pm} 1.30$	1.077
				$\pm 0.89$
Oven	$1.43 \pm 0.016$	$41.3 \pm 1.46$	$52.5 \pm 2.52$	$2.11 \pm 0.63$
Autoclave	$1.42 \pm 0.009$	$40.2 {\pm} 0.45$	$49.89 \pm 0.46$	$1.78 \pm 0.47$

than that of samples cured by oven and autoclave. At the edge position, the tools did not directly heat the sample. The heating is merely from the heat conducted when heating the 1st row in the sample. For the autoclave and oven, this difference is slight as the entire sample is heated. Overall, DPIF shows good uniformity in DoC beyond the first pass of the tool. It could be improved along the first row with repeated passes of the tool, but in a production environment, it would more likely just be removed as scrap to create a net-shape part.

#### 4.10. Mechanical properties

The influence of the different manufacturing methods on the tensile and flexural mechanical properties of CFRP was measured by preparing flat panels and cutting test samples by CNC milling. Panels from the hand-prepared, pre-preg 2x2 twill weave, with 2 wt.% CB was prepared. These were subsequently consolidated and cured using the oven, autoclave or DPIF. Panel thicknesses were 5 layers ( $\sim$ 1 mm) for tensile tests or 15 layers ( $\sim$ 4 mm) for flexural tests were prepared. Samples of dimension  $150\times15\times\sim1$  mm were cut by waterjet for tensile tests and  $80\times13\times\sim4$  mm for the flexural tests.

#### 4.10.1. Tensile properties

The tensile properties (tensile strength and Young's modulus) of CFRP at 1 mm/min are illustrated in Fig. 15. The loading direction is along the fibre in the tensile test. As a result, this is a fibre-dominated property. As expected, there was no statistically significant difference in the tensile strength and Young's modulus of CFRP samples. ANOVA tests show F values of 2.5 and 0.06 for tensile strength and Young's modulus, respectively, with critical F values of 3.48 for a significance level  $\alpha$  of 0.05. Thus, there is no statistically significant difference in

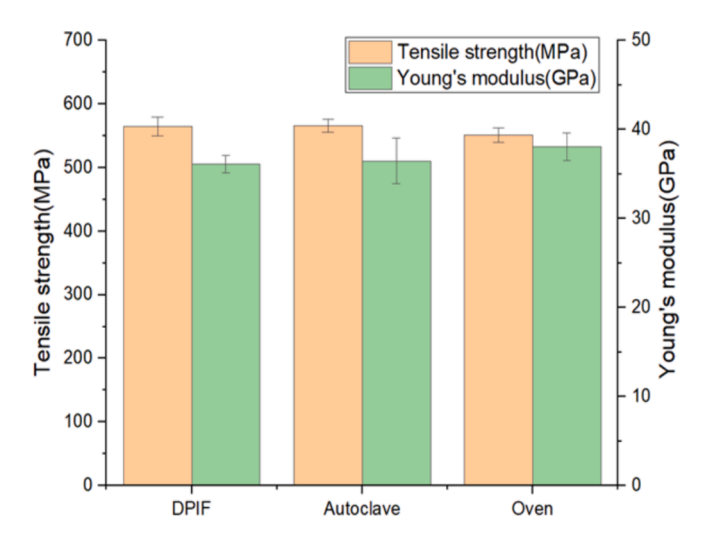


Fig. 15. Comparison of the tensile properties (tensile strength and Young's modulus) of the CFRP+2 wt.% CB samples manufactured using DPIF, autoclave and oven curing methods. The error bar is the standard deviation of five samples.

these samples' tensile strength and Young's modulus. Therefore, DPIF manufacturing does not significantly damage carbon fibre nor degrade its mechanical performance.

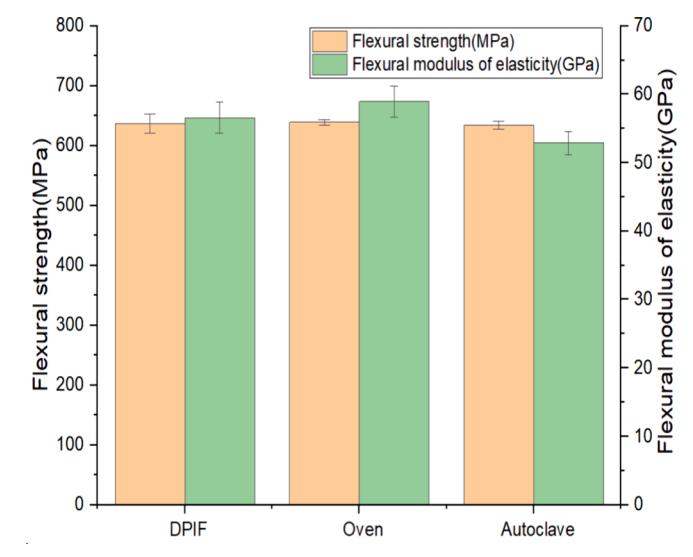
#### 4.10.2. Flexural properties

Fig. 16 shows the flexural properties (flexural strength and flexural modulus of elasticity) of CFRP samples with 2 wt.% CB in the matrix at 1 mm/min. An ANOVA was used to analyse the difference in flexural strength and flexural modulus of 12 samples manufactured by the various methods. For an  $\alpha$  of 0.05, the F values are 2.514 and 0.903 for flexural strength and modulus, respectively. Both values are far lower than the critical F value of 4.07. Therefore, DPIF shows no statistically significant difference in flexural properties compared to the oven and autoclave cure.

# 4.11. Energy consumption

Energy consumption is a crucial economic factor when considering manufacturing operations. It must be recognised that the highest greenhouse gas contribution for CFRP products occurs during the manufacture of the carbon fibre itself. Recent advances in carbon fibre production from bio-sourced PAN have cut this considerably[48]. However, any method that limits greenhouse gas emissions during manufacturing is beneficial. The energy density (J/mm3) of the various manufacturing methods is shown in Fig. 17. Compared to autoclave and oven curing, the energy consumption of DPIF is lower.

Regarding the 15-ply panel (150×150 ×~4 mm), the energy consumption of DPIF is only 4 % and 15 % of that of autoclave and oven, respectively. In addition, compared with a sample with 5 plies, the energy density of a sample with 15 plies increases by 34 % in DPIF, which is significantly lower than the increase in oven and autoclave, at 189 % and 195 %, respectively. As a result, significant energy is expended to heat the ovens and autoclaves instead of the part. In the interest of a fairer comparison, the oven and autoclave can accommodate larger samples. While the energy required by DPIF scales linearly with the sample area, this is not the case for the oven and autoclave. If the maximum sizes of the product that can be manufactured in the autoclave and oven are considered, the largest scale sample in the autoclave is  $700\times1200 \text{ mm}^2$  and for the oven is  $500\times550 \text{ mm}^2$ . The energy density for a 4 mm thick sample of these sizes is 8.54 and 10.75 J/mm<sup>3</sup> for the autoclave and oven, respectively, or 57 % and 71 % compared to DPIF (detail in SI). As a result, purely in terms of energy input for curing,



**Fig. 16.** The flexural properties (flexural strength and modulus) of CFRP with 2 wt.% CB in the matrix manufactured by DPIF, autoclave and oven curing. The error bar is the standard deviation of 4 samples.

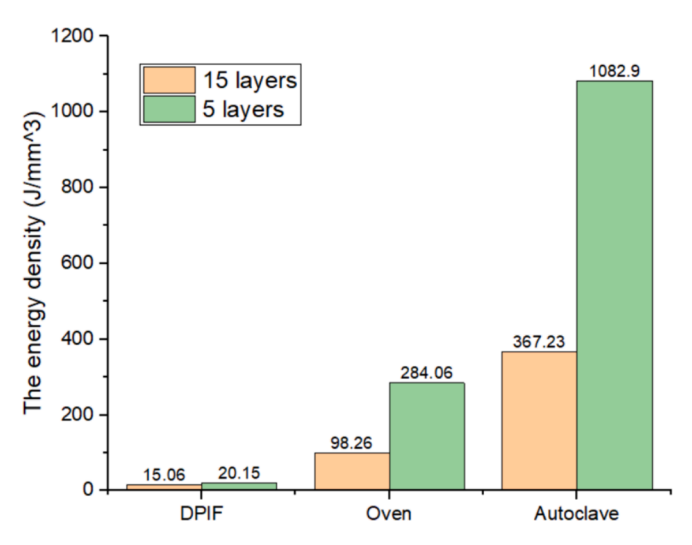


Fig. 17. The energy density of different manufacturing methods (detail in SI).

ovens and autoclaves are cost-effective for manufacturing large-scale products. DPIF is more beneficial for small-scale products. The main advantage of DPIF is the part can be made directly from a computer model without the use of moulds.

#### 5. Conclusion

This study introduces Double-Point Incremental Forming with Direct Electric (Joule) Curing (DPIF-DEC) as a novel and efficient technique for the manufacturing of carbon fibre-reinforced polymer (CFRP). By incorporating 2 wt.% carbon black (CB) into the epoxy resin matrix, electrical conductivity was enhanced, facilitating uniform and rapid curing. The DPIF-DEC process exhibited several significant advantages. Firstly, localised curing is achieved within a short time (40 s) for thick parts (approximately 4 mm). Secondly, the degree of cure (DoC) during the curing process can be controlled and optimised. Mechanical testing shows that DPIF will not damage carbon fibre, and a short, hightemperature curing cycle does not degrade the mechanical performance. Moreover, the energy consumption of DPIF-DEC was significantly lower compared to autoclave and oven curing methods, underscoring the potential of DPIF-DEC as a cost-effective and environmentally sustainable manufacturing method. This study lays a solid foundation for the future application of DPIF-DEC in producing complex, long-fibre composite products without the need for expensive moulds, thereby advancing the field of CFRP manufacturing.

# **Funding statement**

Some of the equipment used in this work was funded through an Engineering and Physical Sciences Research Council grant (EPSRC) Grant number EP/R041733/1.

# CRediT authorship contribution statement

Yunlong Tang: Writing – original draft, Validation, Methodology, Investigation, Formal analysis, Data curation, Conceptualization. J. Patrick A. Fairclough: Writing – review & editing, Writing – original draft, Supervision, Project administration, Funding acquisition.

# Declaration of competing interest

The authors declare that they have no known competing financial interests or personal relationships that could have appeared to influence the work reported in this paper.

#### Data availability

Data will be made available on request.

#### References

- Ahmad F, Al Awadh M, Abas M, Noor S, Hameed A. Optimisation of carbon fiber reinforced plastic curing parameters for aerospace application. Appl Sci 2022;12 (9):4307. https://doi.org/10.3390/appl.2094307.
- [2] Ahmad H, Markina AA, Porotnikov MV, Ahmad F. A review of carbon fiber materials in automotive industry. IOP Conf Ser Mater Sci Eng 2020;971(3):032011. https://doi.org/10.1088/1757-899X/971/3/032011.
- [3] Vijayan DS, Sivasuriyan A, Devarajan P, Stefańska A, Wodzyński Ł, Koda E. Carbon Fibre-Reinforced Polymer (CFRP) Composites in Civil Engineering Application—A Comprehensive Review. Buildings 2023;13(6):1509. https://doi.org/10.3390/ BUIL DINGS13061509
- [4] Vita A, Castorani V, Germani M, Marconi M. Comparative life cycle assessment of low-pressure RTM, compression RTM and high-pressure RTM manufacturing processes to produce CFRP car hoods', in. Procedia CIRP 2019;80:352–7. https:// doi.org/10.1016/i.procir.2019.01.109.
- [5] Van Der Klift F, Koga Y, Todoroki A, Ueda M, Hirano Y, Matsuzaki R. 3D printing of continuous carbon fibre reinforced thermo-plastic (CFRTP) Tensile test specimens. Open J Compos Mater 2016;06(01):18–27. https://doi.org/10.4236/ oicm.2016.61003.
- [6] Mastura MT, Alkahari MR, Syahibudil Ikhwan AK. In: Life cycle analysis of fused filament fabrication: A review. Design for Sustainability. Elsevier; 2021. p. 415–34. https://doi.org/10.1016/B978-0-12-819482-9.00020-4.
- [7] Klosterman D, Chartoff R, Graves G, Osborne N, Priore B. Interfacial characteristics of composites fabricated by laminated object manufacturing. Compos A Appl Sci Manuf 1998;29(9–10):1165–74. https://doi.org/10.1016/S1359-835X(98)00088-
- [8] Karaş B, Smith PJ, Fairclough JPA, Mumtaz K. Additive manufacturing of high density carbon fibre reinforced polymer composites. Addit Manuf 2022;58:103044. https://doi.org/10.1016/j.addma.2022.103044.
- [9] Ramesh M, Rajeshkumar L, Balaji D. Influence of process parameters on the properties of additively manufactured fiber-reinforced polymer composite materials: a review. J Mater Eng Perform 2021;30(7):4792–807. https://doi.org/ 10.1007/s11665-021-05832-y.
- [10] Tekinalp HL, Kunc V, Velez-Garcia GM, Duty CE, Love LJ, Naskar AK, Blue CA, Ozcan S. Highly oriented carbon fiber-polymer composites via additive manufacturing. Compos Sci Technol Dec. 2014;105:144–50. https://doi.org/10.1016/j.compscitech.2014.10.009.
- [11] Justo J, Távara L, García-Guzmán L, París F. Characterisation of 3D printed long fibre reinforced composites. Compos Struct 2018;185:537–48. https://doi.org/ 10.1016/j.compstruct.2017.11.052.
- [12] Handwerker M, Wellnitz J, Marzbani H. Review of mechanical properties of and optimisation methods for continuous fibre-reinforced thermoplastic parts manufactured by fused deposition modelling. Prog Additive Manuf 2021;6(4): 663–77. https://doi.org/10.1007/s40964-021-00187-1.
- [13] Adil S, Lazoglu I. A review on additive manufacturing of carbon fiber-reinforced polymers: Current methods, materials, mechanical properties, applications and challenges. J Appl Polym Sci Feb. 2023;140(7):e53476. https://doi.org/10.1002/ APP.53476.
- [14] Li Y, Chen X, Liu Z, Sun J, Li F, Li J, Zhao G. A review on the recent development of incremental sheet-forming process. Int J Adv Manuf Technol 2017;92(5–8): 2439–62. https://doi.org/10.1007/s00170-017-0251-z.
- [15] Duflou JR, Habraken A-M, Cao J, Malhotra R, Bambach M, Adams D, Vanhove H, Mohammadi A, Jeswiet J. Single point incremental forming: state-of-the-art and prospects. International Journal of Material Forming Nov. 2018;11(6):743–73. htt ps://doi.org/10.1007/s12289-017-1387-y.
- [16] Behera AK, de Sousa RA, Ingarao G, Oleksik V. Single point incremental forming: an assessment of the progress and technology trends from 2005 to 2015. J Manuf Process 2017;27:37–62. https://doi.org/10.1016/j.jmapro.2017.03.014.
- [17] Silva MB, Skjoedt M, Martins PAF, Bay N. Revisiting the fundamentals of single point incremental forming by means of membrane analysis. Int J Mach Tool Manu 2008;48(1):73–83. https://doi.org/10.1016/J.IJMACHTOOLS.2007.07.004.
- [18] Emami R, Mirnia MJ, Elyasi M, Zolfaghari A. An experimental investigation into single point incremental forming of glass fiber-reinforced polyamide sheet with different fiber orientations and volume fractions at elevated temperatures. J Thermoplast Compos Mater 2023;36(5):1893–917. https://doi.org/10.1177/ 000707773077666
- [19] Okada M, Kato T, Otsu M, Tanaka H, Miura T. Development of optical-heating-assisted incremental forming method for CFRTP sheet Fundamental forming characteristics in spot-forming -. Procedia Eng 2017;207:813–8. https://doi.org/10.1016/j.proeng.2017.10.834.
- [20] Cedeno-Campos VM, Jaramillo PA, Fernyhough CM, Fairclough JPA. Towards mould free composites manufacturing of thermoset pre-pregs. Incremental curing with localised pressure-heat (ICULPH). Procedia CIRP 2019;85:237–42. https:// doi.org/10.1016/j.procir.2019.09.020.
- [21] Moser N, Leem D, Ehmann K, Cao J. A high-fidelity simulation of double-sided incremental forming: improving the accuracy by incorporating the effects of machine compliance. J Mater Process Technol 2021;295:117152. https://doi.org/ 10.1016/j.jmatprotec.2021.117152.

- [22] Meier H, Magnus C, Smukala V. Impact of superimposed pressure on dieless incremental sheet metal forming with two moving tools. CIRP Ann 2011;60(1): 327–30. https://doi.org/10.1016/j.cirp.2011.03.134.
- [23] Malhotra R, Cao J, Ren F, Kiridena V, Cedric Xia Z, Reddy NV. Improvement of geometric accuracy in incremental forming by using a squeezing toolpath strategy with two forming tools. J Manuf Sci Eng 2011;133(6). https://doi.org/10.1115/ 1.4005179.
- [24] BuketovA.Smetankin S, Lysenkov E, Yurenin K, Akimov O, Yakushchenko S. Electrophysical properties of epoxy composite materials filled with carbon black nanopowder. Adv Mater Sci Eng 2020. https://doi.org/10.1155/2020/6361485.
- [25] Krieg AS, King JA, Jaszczak DC, Miskoglu I, Mills OP, Odegard GM. Tensile and conductivity properties of epoxy composites containing carbon black and graphene nanoplatelets. J Compos Mater Dec. 2018;52(28):3909–18. https://doi.org/ 10.1177/0021998318771460.
- [26] Fukuda H. Processing of carbon fiber reinforced plastics by means of Joule heating. Adv Compos Mater 1994;3(3):153–61. https://doi.org/10.1163/ 156855194X00015
- [27] Hayes SA, Lafferty AD, Altinkurt G, Wilson PR, Collinson M, Duchene P. Direct electrical cure of carbon fiber composites. Adv Manuf Polym Compos Sci 2015;1 (2):112–9. https://doi.org/10.1179/2055035915Y.0000000001.
- [28] Joseph C, Viney C. Electrical resistance curing of carbon-fibre/epoxy composites. Compos Sci Technol 2000;60(2):315–9. https://doi.org/10.1016/S0266-3538(99) 00112-8.
- [29] Tang Y, Patrick J. Electrical curing of carbon fibre composites with conductive epoxy resins. Compos A Appl Sci Manuf 2024;185:108296. https://doi.org/ 10.1016/J.COMPOSITESA 2024.108296
- [30] Easy Composites Ltd., 'IN2 EPOXY INFUSION RESIN-Technical Datasheet'. https://media.easycomposites.co.uk/datasheets/EC-TDS-IN2-Infusion-Resin.pdf (accessed May 19, 2023).
- [31] Fisher Scientific, 'Carbon black, acetylene, 100% compressed, Thermo Scientific Chemicals'. https://www.fishersci.co.uk/shop/products/carbon-black-acetylene-100-compressed-99-9-thermo-scientific/15406995 (accessed Jul. 12, 2024).
- [32] W. M. Hess and C. R. Herd, 'Microstructure, Morphology and General Physical Properties', in *Carbon Black*, Routledge, 2018, pp. 89–173.
- [33] PYROFIL, 'Typical Properties of carbon fiber'. https://media.easycomposites.co. uk/datasheets/Pyrofil-TRSeries.pdf (accessed Apr. 03, 2024).
- [34] Easy Composites Ltd., '210g Plain Weave 3k Carbon Fibre Cloth'. https://www.eas ycomposites.co.uk/200g-plain-weave-3k-carbon-fibre-cloth (accessed May 19, 2023)
- [35] Wellen RMR, Canedo EL. On the Kissinger equation and the estimate of activation energies for non-isothermal cold crystallisation of PET. Polym Test 2014;40:33–8. https://doi.org/10.1016/J.POLYMERTESTING.2014.08.008.
- [36] Vyazovkin S. Kissinger Method in Kinetics of Materials: Things to Beware and Be Aware of, Molecules 2020;25(12), https://doi.org/10.3390/molecules25122813.

- [37] Schulz H. From the Kissinger equation to model-free kinetics: reaction kinetics of thermally initiated solid-state reactions. ChemTexts 9, Oct. 2018;4(3). https://doi. org/10.1007/s40828-018-0062-3.
- [38] Han S, Chung DDL. Increasing the through-thickness thermal conductivity of carbon fiber polymer-matrix composite by curing pressure increase and filler incorporation. Compos Sci Technol 2011;71(16):1944–52. https://doi.org/ 10.1016/j.compscitech.2011.09.011.
- [39] Li S, Yu X, Bao H, Yang N. High Thermal Conductivity of Bulk Epoxy Resin by Bottom-Up Parallel-Linking and Strain: A Molecular Dynamics Study. The Journal of Physical Chemistry C Jun. 2018;122(24):13140–7. https://doi.org/10.1021/acs. ipcc.8b02001.
- [40] Matsuzaki R, Tachikawa T, Ishizuka J. Estimation of state and material properties during heat-curing molding of composite materials using data assimilation: a numerical study. Heliyon 2018;4:554. https://doi.org/10.1016/j.heliyon.2018. e00554.
- [41] Singh AK, Panda BP, Mohanty S, Nayak SK, Gupta MK. Thermokinetics behavior of epoxy adhesive reinforced with low viscous aliphatic reactive diluent and nanofillers. Korean J Chem Eng 2017;34(11):3028–40. https://doi.org/10.1007/ s11814-017-0221-z.
- [42] Abenojar J, del Real JC, Ballesteros Y, Martinez MA. Kinetics of curing process in carbon/epoxy nano-composites. IOP Conf Ser Mater Sci Eng 2018;369(1):012011. https://doi.org/10.1088/1757-899X/369/1/012011.
- [43] Karami MH, Kalaee MR, Mazinani S, Shakiba M, Shafiei Navid S, Abdouss M, Beig Mohammadi A, Zhao W, Koosha M, Song Z, Li T. Curing kinetics modeling of epoxy modified by fully vulcanised elastomer nanoparticles using rheometry method. Molecules 2022;27(9):2870. https://doi.org/10.3390/molecules27092870.
- [44] Kim SW, Lu MG, Shim MJ. The isothermal cure kinetic of epoxy/amine system analysed by phase change theory. Poly J 1998;30(2):90–4. https://doi.org/ 10.1295/polymj.30.90.
- [45] Hull D, Clyne TW. Thermal behaviour of composites. Introduction Compos Mater 1996;237–70. https://doi.org/10.1017/CB09781139170130.012.
- [46] Collinson MG, Swait TJ, Bower MP, Nuhiji B, Hayes SA. Development and implementation of direct electric cure of plain weave CFRP composites for aerospace. Compos A Appl Sci Manuf 2023;172:107615. https://doi.org/10.1016/ i.compositesa.2023.107615.
- [47] Liu S, Li Y, Shen Y, Lu Y. Mechanical performance of carbon fiber/epoxy composites cured by self-resistance electric heating method. Int J Adv Manuf Technol 2019;103(9–12):3479–93. https://doi.org/10.1007/s00170-019-03707-0.
- [48] Le ND, Varley RJ, Hummel M, Trogen M, Byrne N. A review of future directions in the development of sustainable carbon fiber from bio-based precursors. Mater Today Sustain 2022;20:100251. https://doi.org/10.1016/J. MTSUST.2022.100251.